

Article

A Curved Plate-Flattening Method to Construct the Membrane Strain Distribution

Lichun Chang ¹, Yao Zhao ^{1,2,*}, Hua Yuan ^{1,2} and Zhenshuai Wei ¹

¹ School of Naval Architecture and Ocean Engineering, Huazhong University of Science and Technology, Wuhan 430074, China

² Hubei Key Laboratory of Naval Architecture and Ocean Engineering Hydrodynamics (HUST), Wuhan 430074, China

* Correspondence: yzhaozzz@hust.edu.cn

Abstract: The surface-flattening process has many applications in industries such as shipbuilding. Curved surfaces in the industry are usually formed from flat surfaces, so the target surface needs to be flattened to obtain its corresponding initial shape. In addition, the surface flattening process obtains the inherent strain distribution required in forming. Different forming methods in the plate forming process will produce different membrane deformations, such as shrinkage in the line heating and tensile in the roller forming. Therefore, different surface-flattening methods should be used to obtain the inherent strain distribution suitable for different forming methods. This paper proposes a method to perform the surface flattening using the finite element method and constrain the membrane strain generated in the flattening deformation by modifying the material constitutive relationship. Using a dual modulus material constitutive model in membrane deformation makes the surface more inclined to deform at locations with less stiffness during the flattening process. This method yields predominantly tensile or compressive membrane strain without changing the bending strain. By modifying the material model, this method can control the compressive strain region and the principal strain direction. The results of the proposed method applying to different surface shapes and its application in the surface-forming process are given in this paper.

Keywords: surface flattening, dual modulus material, inherent strain distribution, plate forming, shell finite element



Citation: Chang, L.; Zhao, Y.; Yuan, H.; Wei, Z. A Curved Plate-Flattening Method to Construct the Membrane Strain Distribution. *J. Mar. Sci. Eng.* **2023**, *11*, 439. <https://doi.org/10.3390/jmse11020439>

Academic Editor: Sergei Chernyi

Received: 20 January 2023

Revised: 13 February 2023

Accepted: 14 February 2023

Published: 16 February 2023



Copyright: © 2023 by the authors. Licensee MDPI, Basel, Switzerland. This article is an open access article distributed under the terms and conditions of the Creative Commons Attribution (CC BY) license (<https://creativecommons.org/licenses/by/4.0/>).

1. Introduction

In engineering, spatial surfaces are usually obtained from two-dimensional flat surfaces. The surface flattening is to find the initial configuration. Meanwhile, surface flattening is an effective method to formulate the forming plan [1,2].

The plate-forming process in the shipbuilding process includes different methods, such as rolling, line heating, and peening. The traditional forming process is mainly based on the workers' experience, but the automated processing requires computerizing the forming process design. The inherent strain is an important parameter to describe the forming process [3]. The inherent strain is the plastic strain induced in the forming process and causes the deformation. The forming process designing is to decide the position of the forming line and the magnitude of the inherent strain. The primary purpose of flattening is to obtain the total inherent strain distribution desired in forming, helping the forming process design.

Different forming methods have different characteristics. For example, rollers cause tensile inherent strain [4], and line-heating processing causes compressive inherent strain [5,6]. The forming method should determine the flattening method. For example, the surface flattening for the roller process should obtain a shrinkage-dominant membrane strain. The surface flattening for the line-heating process should obtain the membrane strain mainly by stretching.

Wang [7] given an example of applying the plate flattening in heating path design. They placed the target surface between two rigid plates; the bottom rigid plate is stationary, and the top rigid plate moves downward with a certain speed. The motion stops when the target surfaces are pressed to a flat plane. They assumed that the plate is isotropic, and did not consider that the line-heating process only produces shrinkage-inherent strain.

Ueda [2] proposed a method for calculating surface flattening using finite elastic elements by applying forced displacements and obtaining the strain distribution after flattening. They made the tensile strain in the final strain distribution as small as possible by iteratively applying initial stress to fit the line heating process. Moreover, it shows that the strain can be concentrated along the direction of the coordinate system or within a specific width by modifying the material elasticity modulus. The results also suggest that the relationship between strain and surface shape is geometrical and unrelated to physical processes. However, this method was mainly proposed for the line heating process, and it should also be noted that this flattening method requires multiple iterations and consumes much computational time.

Ryu [8] introduced an optimal approximate flattening algorithm for double-curved surfaces. This method minimizes the deformation energy from the planar configuration to the desired surface with the constraint of principal strain. In this nonlinearly constrained optimization problem, design variables are nodal coordinates of elements in the flattening plane. Moreover, they assigned constraints to strain following forming methods.

Zhang [9] proposed a method using the SQP optimization algorithm to solve the flattening of double-curved surfaces, similar to Ryu's method. However, they used the result of geometric flattening as the initial value of the optimization algorithm iteration to increase the convergence speed. In addition, they adopted the triangle element strain theory. However, this optimization calculation is still computationally intensive.

Lan [10] proposed an optimization model for flattening of three-dimensional curved hull plates based on an flattening method with a constant unit length. The error of area, linear degree of borders, and mean strain energy were taken as objective functions. The multi-objective memetic algorithm with heuristic operator was adopted to solve the optimization model. This method mainly focuses on the flattening shape.

This paper proposes an efficient method for calculating the flattening of double-curved surfaces using the finite element method to obtain the desired inherent strain in forming. This method can obtain different strain distributions adapted to different forming methods. As generating both tensile and compressive membrane strain during forming is generally impossible, the inherent strain distribution desired for forming should only contain tensile or compressive strain for a specific forming method. The obtained strain distribution is useful in the forming plan design. This paper presents the results for different surface shapes and examples of the application of this method to forming curved plates.

2. Basic Theory and Strategy

This paper uses a mechanical method based on shell finite element theory for surface-flattening calculation. Firstly, build the finite element model of the target surface. The surface is flattened on the plane by applying forced displacement in one direction, with no constraint perpendicular to the forced displacement. It can be deformed arbitrarily in the plane.

The core idea of controlling strain distribution is constructing a material constitutive relationship with dual modulus in tension and compression. So, the membrane component tends to deform more towards the side with the lower stiffness, resulting in a membrane strain distribution which is predominantly tensile or compressive. Moreover, by modifying the membrane shear stiffness, the principal membrane strain is distributed in a specific direction, more conducive to designing the forming plan and performing the automated forming. We have written a program to implement this method of surface flattening. This method obtains the shape of the surface after flattening and the strain generated during the deformation. Figure 1 shows the basic strategy.

It is important to emphasize that surface flattening differs from the actual forming process. The surface flattening process is a means to obtain the inherent strain distribution rather than an actual physical process. Moreover, the relationship between deformation and strain during the flattening process is determined by the continuity condition, independent of the material constitutive relationship. We can consider the total strain obtained in the surface flattening to be the inherent strain required for forming. Therefore, we can simplify the calculation by considering only the elastic process in the calculation.

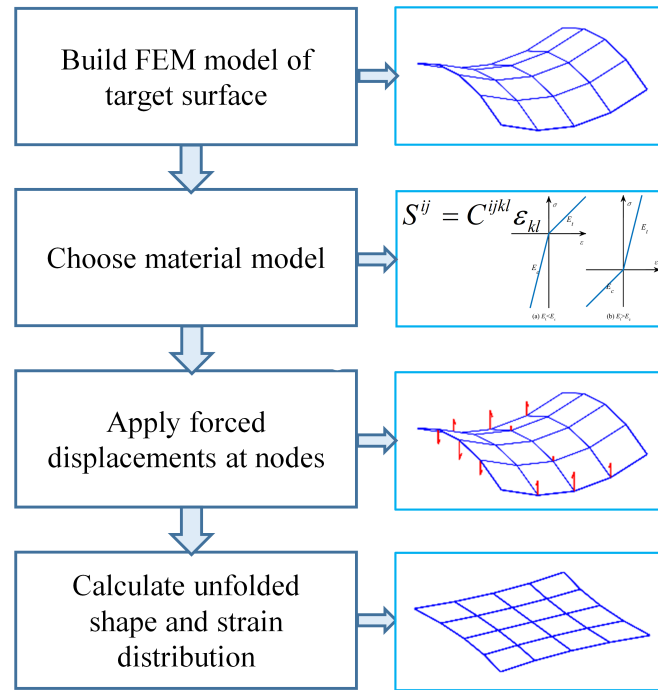


Figure 1. Basic strategy of flattening.

2.1. Shell Mathematical Models

First, let us briefly review the notation, following the usual approach [11]. We denote the 2D tensor by symbols with a number of underscores corresponding to their order and the 3D tensor by symbols over arrows. Note that we use Greek indices, which will implicitly vary in (1, 2), for the components of surface tensors. As shown in Figure 2, $(\vec{x}_1, \vec{x}_2, \vec{x}_3)$ denote the reference orthonormal basis, $(\zeta^1, \zeta^2, \zeta^3)$ denote the curvilinear coordinates of the middle surface. \underline{a} , \underline{b} and \underline{c} refer to the middle surface’s first, second, and third fundamental form. We will use the Einstein summation convention.

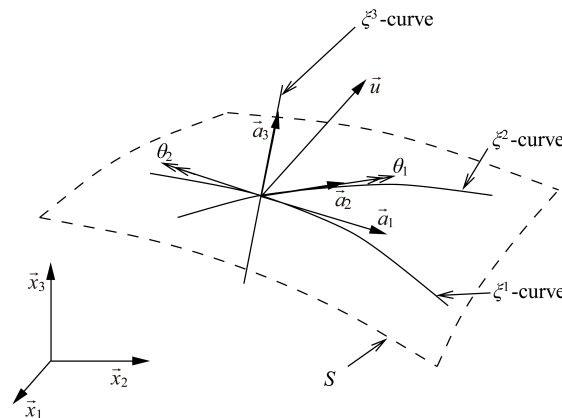


Figure 2. Coordinates of a shell surface.

The geometry of the shell at time t is defined as Equation (1):

$${}^t\vec{X}(\zeta^1, \zeta^2, \zeta^3) = {}^t\vec{x}(\zeta^1, \zeta^2) + \zeta^3 {}^t\vec{a}_3(\zeta^1, \zeta^2). \tag{1}$$

Note that the notation (\vec{a}_1, \vec{a}_2) is the basis of the middle surface, defined in Equation (2). \vec{a}_3 is the unit normal vector, defined in Equation (3). See Figure 2.

$${}^t\vec{a}_\alpha = \frac{\partial {}^t\vec{x}(\zeta^1, \zeta^2)}{\partial \zeta^\alpha}, \tag{2}$$

$${}^t\vec{a}_3 = \frac{{}^t\vec{a}_\alpha \times {}^t\vec{a}_\beta}{\|{}^t\vec{a}_\alpha \times {}^t\vec{a}_\beta\|}. \tag{3}$$

$(\vec{g}_1, \vec{g}_2, \vec{g}_3)$ are the covariant basis of the shell domain, ${}^t\vec{g}_i = \frac{\partial {}^t\vec{X}}{\partial \zeta^i}$.

Moreover, substitute Equation (1) to obtain Equations (4) and (5)

$${}^t\vec{g}_\alpha = (\delta_\alpha^\lambda - \zeta^3 b_\alpha^\lambda) {}^t\vec{a}_\lambda, \tag{4}$$

$${}^t\vec{g}_3 = {}^t\vec{a}_3. \tag{5}$$

The incremental displacement from the configuration at the time t to the configuration at the time $t + \Delta t$ is:

$$\vec{U}(\zeta^1, \zeta^2, \zeta^3) = {}^{t+\Delta t}\vec{X}(\zeta^1, \zeta^2, \zeta^3) - {}^t\vec{X}(\zeta^1, \zeta^2, \zeta^3). \tag{6}$$

A general displacement field can be expressed in Equations (7)–(9):

$$\vec{U}(\zeta^1, \zeta^2, \zeta^3) = \vec{u}(\zeta^1, \zeta^2) + \zeta^3 \theta_\lambda(\zeta^1, \zeta^2) \vec{a}^\lambda(\zeta^1, \zeta^2), \tag{7}$$

with

$$\vec{U}(\zeta^1, \zeta^2, \zeta^3) = \vec{u}(\zeta^1, \zeta^2) + \zeta^3 \theta_\lambda(\zeta^1, \zeta^2) \vec{a}^\lambda(\zeta^1, \zeta^2). \tag{8}$$

Within the scope of the thin shell, the rotation of the straight material line is uniquely defined by a rotation vector normal to that line.

$$\theta_\lambda(\zeta^1, \zeta^2) \vec{a}^\lambda(\zeta^1, \zeta^2) = {}^{t+\Delta t}\vec{a}_3(\zeta^1, \zeta^2) - {}^t\vec{a}_3(\zeta^1, \zeta^2). \tag{9}$$

Hence, \vec{u} denotes the middle-surface displacement solution and θ denotes the rotation solution. The covariant Green–Lagrange strain components at the time t and referred to at time 0 are defined by Equation (10)

$${}^t\varepsilon_{ij}(\zeta^1, \zeta^2, \zeta^3) = \frac{1}{2}({}^t\vec{g}_i \cdot {}^t\vec{g}_j - {}^0\vec{g}_i \cdot {}^0\vec{g}_j). \tag{10}$$

The incremental covariant strain components are

$$\begin{aligned} \varepsilon_{ij}(\zeta^1, \zeta^2, \zeta^3) &= {}^{t+\Delta t}\varepsilon_{ij}(\zeta^1, \zeta^2, \zeta^3) - {}^t\varepsilon_{ij}(\zeta^1, \zeta^2, \zeta^3) \\ &= \frac{1}{2}({}^t\vec{g}_i \cdot \vec{U}_{,j} + \vec{U}_{,i} \cdot {}^t\vec{g}_j + \vec{U}_{,i} \cdot \vec{U}_{,j}), \end{aligned} \tag{11}$$

with $\vec{U}_{,i} = \frac{\partial \vec{U}}{\partial \zeta^i}$.

The principle of virtual work applied to the configuration at the time $t + \Delta t$ is [12]:

$$\int_V {}^{t+\Delta t}S^{ij} \delta {}^{t+\Delta t}\varepsilon_{ij} dV = W, \tag{12}$$

where the ${}^{t+\Delta t}S^{ij}$ are the contravariant components of the second Piola–Kirchhoff stress tensor at the time $t + \Delta t$ and referred to the configuration at the time 0, and the ${}^{t+\Delta t}\varepsilon_{ij}$ are

the covariant components of the Green–Lagrange strain tensor at the time $t + \Delta t$ and refer to the time 0. The external virtual work is given by W and includes the work due to the applied surface tractions and body forces.

We have the appropriate constitutive relations:

$$S^{ij} = C^{ijkl} \varepsilon_{kl}, \tag{13}$$

where C^{ijkl} is the contravariant constitutive tensor in the natural coordinates.

In mathematics, double-curved surfaces do not have isometric correspondence with a flat surface. Therefore, it cannot be deformed from the flat plate to the non-developable surface without stretching, compression, or wrinkles. In the double-curved surface-forming process, both membrane deformation and bending deformation must be applied. The bending deformation is determined by the local curvature of the surface, while the overall curvature inhomogeneity determines membrane deformation. We purpose to construct the membrane strain distribution by changing the constitutive relation tensor while not willing to affect the bending strain. Therefore, we divide the total strain into the membrane and bending strain. We need to force the curved shell deformed to the plane by forced displacement, so the external loads should be zero, $W = 0$. In addition, we consider the thickness of the shell as a constant. From Equations (10) and (11), we obtain the expression of each strain component:

$$\begin{cases} \varepsilon_{\alpha\beta} &= (m)\varepsilon_{\alpha\beta} + (b)\varepsilon_{\alpha\beta} \quad \alpha, \beta = 1, 2, \\ \varepsilon_{\alpha 3} &= \frac{1}{2} ({}^t\vec{g}_\alpha \cdot \theta_\lambda \vec{a}^\lambda + {}^t\vec{a}_3 \cdot \vec{U}_{,\alpha} + \theta_\lambda \vec{a}^\lambda \cdot \vec{U}_{,\alpha}), \\ \varepsilon_{33} &= 0, \end{cases} \tag{14}$$

with

$$\begin{cases} (m)\varepsilon_{\alpha\beta} &= \frac{1}{2} (\vec{a}_\alpha \cdot \vec{u}_{,\beta} + \vec{a}_\beta \cdot \vec{u}_{,\alpha} + \vec{u}_{,\alpha} \cdot \vec{u}_{,\beta}), \\ (b)\varepsilon_{\alpha\beta} &= \frac{1}{2} \zeta^3 (b_\alpha^\lambda \vec{a}_\lambda \cdot \vec{u}_{,\beta} + b_\beta^\lambda \vec{a}_\lambda \cdot \vec{u}_{,\alpha} \\ &\quad + \vec{a}_\alpha \cdot \frac{\partial(\theta_\lambda \vec{a}^\lambda)}{\partial \zeta^\beta} + \vec{a}_\beta \cdot \frac{\partial(\theta_\lambda \vec{a}^\lambda)}{\partial \zeta^\alpha} \\ &\quad + \frac{\partial(\theta_\lambda \vec{a}^\lambda)}{\partial \zeta^\alpha} \cdot \vec{u}_{,\beta} + \frac{\partial(\theta_\lambda \vec{a}^\lambda)}{\partial \zeta^\beta} \cdot \vec{u}_{,\alpha}) \\ &\quad + \frac{1}{2} (\zeta^3)^2 (b_\alpha^\lambda \vec{a}_\lambda \cdot \frac{\partial(\theta_\lambda \vec{a}^\lambda)}{\partial \zeta^\beta} \\ &\quad + b_\beta^\lambda \vec{a}_\lambda \cdot \frac{\partial(\theta_\lambda \vec{a}^\lambda)}{\partial \zeta^\alpha} \\ &\quad + \frac{\partial(\theta_\lambda \vec{a}^\lambda)}{\partial \zeta^\alpha} \cdot \frac{\partial(\theta_\lambda \vec{a}^\lambda)}{\partial \zeta^\beta}). \end{cases} \tag{15}$$

Moreover, from surface theory, we have:

$$\begin{cases} \vec{u}_{,\alpha} = \frac{\partial \vec{u}}{\partial \zeta^\alpha} = (u_{\lambda\alpha} - b_{\lambda\alpha} u_3) \vec{a}^\lambda + (u_{3,\alpha} + b_\alpha^\lambda u_\lambda) \vec{a}_3, \\ \frac{\partial(\theta_\lambda \vec{a}^\lambda)}{\partial \zeta^\alpha} = \theta_{\lambda\beta} \vec{a}^\lambda + b_\alpha^\lambda \theta_\lambda \vec{a}_3. \end{cases} \tag{16}$$

Respectively, we separate the corresponding stress in Equation (13):

$$\begin{cases} (m)S^{\alpha\beta} &= (m)C^{\alpha\beta\lambda\mu} (m)\varepsilon_{\lambda\mu}, \\ (b)S^{\alpha\beta} &= (b)C^{\alpha\beta\lambda\mu} (b)\varepsilon_{\lambda\mu}, \\ S^{\alpha 3} &= \frac{1}{2} D^{\alpha\lambda} \varepsilon_{\lambda 3}, \end{cases} \tag{17}$$

where $(m)S^{\alpha\beta}, (b)S^{\alpha\beta}, S^{\alpha 3}$ represent membrane stress, bending stress, and transverse shear stress, respectively.

Consider an isotropic linear elastic material following Hooke’s law for bending strain:

$$(b)C^{\alpha\beta\lambda\mu} = \frac{E}{2(1 + \nu)} (a^{\alpha\lambda} a^{\beta\mu} + a^{\alpha\mu} a^{\beta\lambda} + \frac{2\nu}{1 - \nu} a^{\alpha\beta} a^{\lambda\mu}) \tag{18}$$

$$D^{\alpha\lambda} = \frac{2E}{1 + \nu} a^{\alpha\lambda} \tag{19}$$

where we classically denote Young’s modulus by E and Poisson’s ratio by ν . $(b)C^{\alpha\beta\lambda\mu}$ refers to the constitutive tensor in natural coordinate for bending strain and $D^{\alpha\lambda}$ refers to the constitutive tensor in natural coordinate for transverse shear strain.

As mentioned before, we must use different constitutive relationships for membrane strain in different situations. The following sections introduce different constitutive relations used to constrain membrane strain distribution.

2.2. Constrain the Magnitude of Membrane Strain

In the plate-forming process, generating both compressive and tensile membrane strain is often impossible. Since the surface-flattening process is designed to obtain the inherent strain required in forming, we need to generate only compressive or tensile membrane strain during surface flattening.

Therefore, we modify the material’s constitutive relationship to control the strain distribution obtained by surface flattening. When we need to obtain a predominant compressive membrane strain, we reduce the material’s stiffness in compression, constructing a material constitutive relation that satisfies the condition $E_c < E_t$. E_t represents Young’s modulus in tension and E_c represents Young’s modulus in compression, so that the material fibers are more inclined to produce compressive deformation, we must adopt a material constitutive relationship with different tensile and compressive moduli, also called a dual modulus material, see Figure 3.

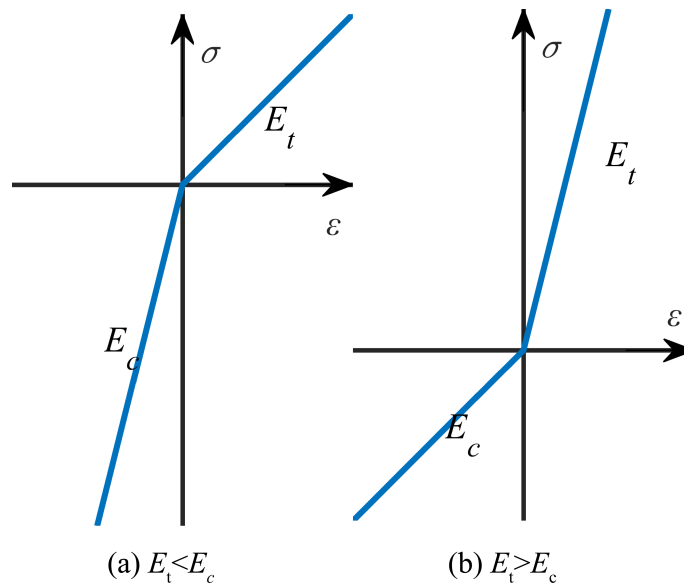


Figure 3. Dual modulus stress–strain relation (a) $E_t < E_c$, (b) $E_t > E_c$.

In an arbitrary cross-section on a surface, the internal forces in the cross section must be equilibrium since there are no external forces on the surface during the flattening process, as in Figure 4. When using isotropic material properties, the magnitude of the tensile strain is close to that of the compressive strain due to the requirement of internal force balance. When the material stiffness in the tensile region decreases, the tensile strain increases to ensure the internal force equilibrium. Again, the compressive strain will decrease due to the requirement of deformation continuity. This also means that the tensile strain zone expands while the compressive strain zone reduces. For any cross-section, this process exists, and the final strain distribution obtained is predominant tensile. Based on the above principles, we use a dual-modulus material model to achieve control of the strain magnitude.

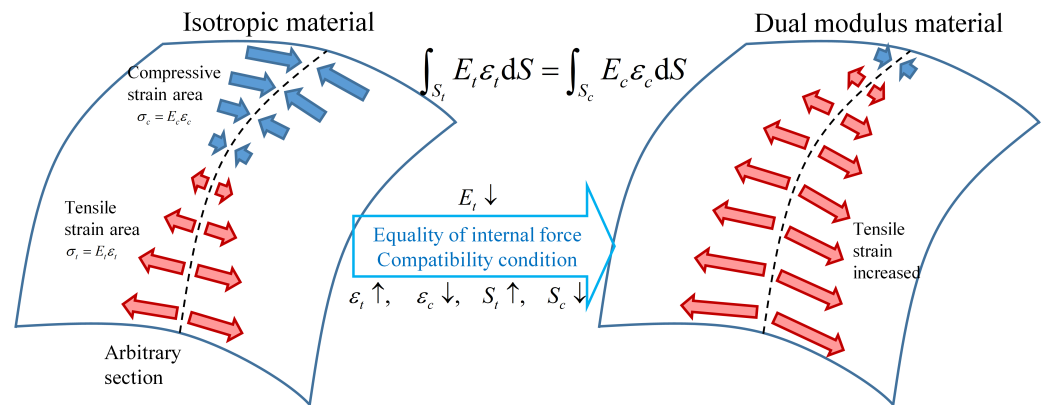


Figure 4. Constrain the magnitude of membrane strain.

To analyze the material with different modules in tension and compression, Ambartsumyan [13,14] defined a set of stress–strain relations referred to herein as the Ambartsumyan material model. Tabaddor [15] elaborated somewhat on the Ambartsumyan material model. Jones [16,17] applied the model to the problem of buckling under biaxial loading of circular cylindrical shells made of isotropic material.

According to the Ambartsumyan material model, the material’s constitutive relation is determined by the principal stress state. $(_{(p)}\vec{a}_1, _{(p)}\vec{a}_2)$ denote the principal direction of the membrane strain in the tangent plane of the middle surface. We use $_{(p)}\gamma_{\alpha\beta}$ to represent the principal membrane strain component. $_{(pm)}C^{\alpha\beta\lambda\mu}$ represent the constitutive components in the principal direction. Then we have the following equations:

$$_{(p)}\vec{a}_\alpha \cdot \vec{a}_3 = _{(p)}\vec{a}_\alpha \cdot \vec{a}^3 = 0, \tag{20}$$

$$_{(p)}\vec{a}_1 \cdot _{(p)}\vec{a}_2 = 0, \tag{21}$$

$$\|_{(p)}\vec{a}_1\| = \|_{(p)}\vec{a}_2\| = 1. \tag{22}$$

We use the left subscript (p) to represent the principal direction.

It is well known that the principal strain $_{(p)}\gamma_{\alpha\alpha}$ is the eigenvalue of the strain’s mixed component γ_α^β . We can obtain the principal membrane strain $_{(p)}\gamma$ and the principal direction $_{(p)}\vec{a}_\alpha = j_\alpha^\beta \vec{a}_\beta$ by solving the eigenvalues and the eigenvectors.

$$\det(\gamma_\alpha^\beta - _{(p)}\gamma \delta_\alpha^\beta) = 0, \tag{23}$$

$$(\gamma_\alpha^\beta - _{(p)}\gamma \delta_\alpha^\beta) j^\alpha = 0. \tag{24}$$

Then we can transform the constitutive components from the principal direction to the natural direction basis [18]. $_{(m)}C^{\alpha\beta\lambda\mu}$ refers to the constitutive tensor in the natural coordinate for membrane strain.

$$_{(m)}C^{\alpha\beta\lambda\mu} = (\vec{a}^\alpha \cdot _{(p)}\vec{a}_{\alpha'}) (\vec{a}^\beta \cdot _{(p)}\vec{a}_{\beta'}) (\vec{a}^\lambda \cdot _{(p)}\vec{a}_{\lambda'}) (\vec{a}^\mu \cdot _{(p)}\vec{a}_{\mu'}) _{(pm)}C^{\alpha'\beta'\lambda'\mu'} \tag{25}$$

To avoid the effect between the two principal directions, we ignore the Poisson effect in the classical elastic material, so we let $\nu = 0$. Then we have

$$\begin{aligned} {}_{(pm)}C^{\alpha\alpha\alpha\beta} &= {}_{(pm)}C^{\alpha\alpha\beta\alpha} \\ &= {}_{(pm)}C^{\alpha\beta\alpha\alpha} = {}_{(pm)}C^{\beta\alpha\alpha\alpha} \\ &= {}_{(pm)}C^{\alpha\alpha\beta\beta} = 0 \quad (\text{when } \alpha \neq \beta) \end{aligned} \tag{26}$$

$${}_{(pm)}C^{\alpha\alpha\alpha\alpha} = \begin{cases} E_c & \text{if } {}_{(p)}\gamma_{\alpha\alpha} \leq 0 \\ E_t & \text{if } {}_{(p)}\gamma_{\alpha\alpha} > 0 \end{cases} \tag{27}$$

where E_c, E_t represent the compressive and tensile moduli, respectively.

To ensure convergence, we let

$${}_{(pm)}C^{\alpha\beta\alpha\beta} = {}_{(pm)}C^{\alpha\beta\beta\alpha} = \frac{{}_{(pm)}C^{1111} {}_{(pm)}C^{2222}}{{}_{(pm)}C^{1111} + {}_{(pm)}C^{2222}} \quad (\text{when } \alpha \neq \beta) \tag{28}$$

as He [19] suggested.

We let $E_c = nE$ and $E_t = E$ with $0 < n < 1$ when we want to obtain a strain distribution dominated by compressive strain. We may refer to n as the relaxation factor. The factor n is an imagined value used to construct the dual modulus material. When n is small, the tensile stress generated will be much greater than compressive. It is much easier to produce compressive strain and vice versa. On the contrary, we let $E_t = nE$ and $E_c = E$ with $0 < n < 1$, when we want to obtain a strain distribution dominated by tensile strain. Furthermore, we can control the ratio of the area of the compressive area and the tensile area by changing the value of the relaxation factor n .

2.3. Constrain the Direction of Membrane Strain

We need to specify this direction in advance when we want the principal strain to be distributed only in a specified direction, for example, orthogonal to the Cartesian coordinate axis. Then we define a material constitutive relationship in this specified direction to reinforce the shear stiffness along this direction. It is not easy to produce shear deformation in this direction when the forced displacement is applied. When the shear strain in the principal direction of the material is slight, the principal direction of the strain is nearly the same as the principal direction of the material, and the principal strain distributes in the specified direction.

We use $({}_{(c)}\vec{a}_1, {}_{(c)}\vec{a}_2)$ to represent the constrained strain direction needed. Similarly to Equation (25), we have

$${}_{(m)}C^{\alpha\beta\lambda\mu} = (\vec{a}^\alpha \cdot {}_{(c)}\vec{a}_{\alpha'}) (\vec{a}^\beta \cdot {}_{(c)}\vec{a}_{\beta'}) (\vec{a}^\lambda \cdot {}_{(c)}\vec{a}_{\lambda'}) (\vec{a}^\mu \cdot {}_{(c)}\vec{a}_{\mu'}) {}_{(cm)}C^{\alpha'\beta'\lambda'\mu'} \tag{29}$$

where ${}_{(cm)}C^{\alpha\beta\lambda\mu}$ denotes the constitutive components of membrane strain in the specified constrained direction. We use the left subscript (c) to represent the constrained direction.

Similarly, we define the constitutive components as follows:

$$\left\{ \begin{aligned} &{}_{(cm)}C^{\alpha\alpha\alpha\beta} = {}_{(cm)}C^{\alpha\alpha\beta\alpha} \\ &= {}_{(cm)}C^{\alpha\beta\alpha\alpha} = {}_{(cm)}C^{\beta\alpha\alpha\alpha} \\ &= {}_{(cm)}C^{\alpha\alpha\beta\beta} = 0 \quad (\text{when } \alpha \neq \beta), \\ &{}_{(cm)}C^{\alpha\alpha\alpha\alpha} = E, \\ &{}_{(cm)}C^{\alpha\beta\alpha\beta} = {}_{(cm)}C^{\alpha\beta\beta\alpha} = \frac{mE}{2}, \\ &\text{with } m > 1 \quad (\text{when } \alpha \neq \beta). \end{aligned} \right. \tag{30}$$

In this constitutive relationship, since we reinforce the shear stiffness along this direction, the membrane strain is generated in the specified direction during the deformation of

the surface flattening. This way, we can obtain a more regular membrane strain distribution, which is beneficial for forming plan design.

Furthermore, we can combine these two conditions, Equations (26)–(28) and (30).

$$\left\{ \begin{array}{l} {}_{(cm)}C^{\alpha\alpha\alpha\beta} = {}_{(cm)}C^{\alpha\alpha\beta\alpha} \\ \quad = {}_{(cm)}C^{\alpha\beta\alpha\alpha} = {}_{(cm)}C^{\beta\alpha\alpha\alpha} \\ \quad = {}_{(cm)}C^{\alpha\alpha\beta\beta} = 0 \quad (\text{when } \alpha \neq \beta), \\ {}_{(cm)}C^{\alpha\alpha\alpha\alpha} = \begin{cases} E_c & \text{if } {}_{(c)}\gamma_{\alpha\alpha} \leq 0 \\ E_t & \text{if } {}_{(c)}\gamma_{\alpha\alpha} > 0 \end{cases} , \\ {}_{(cm)}C^{\alpha\beta\alpha\beta} = {}_{(cm)}C^{\alpha\beta\beta\alpha} \\ \quad = \frac{m {}_{(cm)}C^{1111} {}_{(cm)}C^{2222}}{{}_{(cm)}C^{1111} + {}_{(cm)}C^{2222}} , \\ \text{with } m > 1 \quad (\text{when } \alpha \neq \beta). \end{array} \right. \quad (31)$$

Using the constitutive relationship above, we can obtain the membrane strain in a specific direction. When we want to obtain a strain distribution dominated by compressive strain, we let $E_c = nE$ and $E_t = E$ with $0 < n < 1$.

Based on the above model, discretize the target surface. We can carry out the stiffness matrix by using the constitutive relationship above and applying the virtual work principle. We can obtain the displacement field solution and the flattened shape by solving the equilibrium equations. Then, employing Equation (15), the membrane and bending strain distribution are obtained. In addition, due to the continuity of the displacement field, the compatibility condition is satisfied naturally.

3. Numerical Example

Much research has been published on shell finite elements. We use MITC4 (mixed interpolation of tensorial components) [12,20] elements to discretize the shells and solve the problems. In this section, we write programs to implement the above flattening method and give examples of calculations for different double-curved surfaces flattening.

3.1. Spherical Cap

We use a spherical cap with a curvature of 1 m^{-1} and a radius of 0.6 m as the target shape for the surface-flattening calculation, shown in Figure 5. This section calculates the membrane strain dominated by compressive or tension according to the above algorithm and compares the differences in the results when the relaxation factor n is taken at different values.

In this comparison, the result of surface flattening using isotropic general steel constitutive relations is the reference result. It can be found that the circumferential strain is tensile strain, and the radial strain is compressive strain near the edge. This form of strain distribution is difficult to achieve in a usual forming process. Following the above method, we need to constrain the strain magnitude generated by the surface flattening. The stiffness in one direction reduces by using the relaxation factor n described above. The relaxation factor n takes the values of 0.1, 0.01, and 0.001, respectively, to compare their calculation results.

Figure 6 shows the membrane strain distribution dominated by tensile strain, (a) for the reference result and (b), (c), and (d) for the conditions $n = 0.1, 0.01,$ and $0.001,$ respectively. Figure 7 shows the membrane strain distribution dominated by compressive strain. Take the circumferential and radial strain on a radius and compare their distribution in the radial direction, as shown in Figure 8. Moreover, Table 1 compares the flattened surface’s shape and the membrane strain’s value.

In the reference result, we obtain tensile strain near the edges and compressive strain near the center. The maximum values of both are similar. When we constrain the membrane strain to obtain compressive strain, in the condition $n = 0.1,$ it can be seen from the figure

that the area of the contracted part of the center of the spherical cap increases significantly. The tensile strain near the edge decreases, but a part of the area in the tensile state remains. When $n = 0.01$, the compressive strain on the surface continues to increase. At this time, the tensile strain on the surface is already significantly smaller than the compressive strain. Finally, when n decreases to 0.001, the compressive strain in the surface increases slightly. At this point, the surface is in a contracted state, and in the edge area, there is still a tensile circumferential strain.

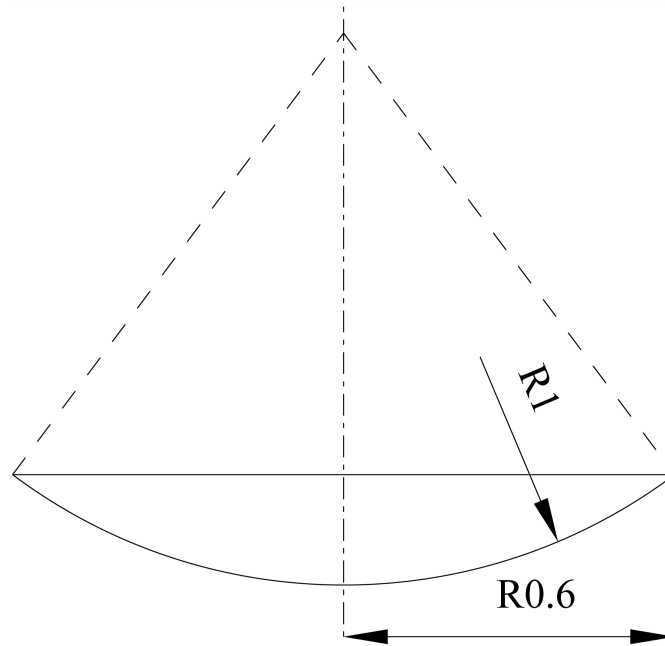


Figure 5. The dimension of the spherical cap.

Table 1. Comparison of spherical cap shape-flattening results.

Case		Radius after Flattening	Change Relative to the Original Arc Length (%)	The Radius of the Compressive Area	Maximum Membrane Strain	Minimum Membrane Strain
Compressive	$n = 0.001$	0.606	-5.9	0.606	0.0072	-0.0679
	$n = 0.01$	0.608	-5.5	0.608	0.0105	-0.0647
	$n = 0.1$	0.618	-4.0	0.577	0.0236	-0.0512
Reference		0.632	-1.7	0.451	0.0437	-0.0269
Tensile	$n = 0.1$	0.641	-0.4	0.266	0.0565	-0.0089
	$n = 0.01$	0.644	0.0	0.143	0.0601	-0.0025
	$n = 0.001$	0.644	0.1	0.103	0.0611	-0.0013

Similarly, when we constrain the membrane strain to obtain tensile strain, the shrinkage region near the center of the surface gradually reduces as the relaxation factor n decreases. When $n = 0.001$, the shrinkage strain exists only within a radius of 0.1 m and is numerically much smaller than the tensile strain. Moreover, Table 1 shows that when flattening the surface to compress, the radius after flattening is 5.9% smaller than the arc length of the surface. In contrast, when flattening the surface to stretch, the radius after flattening is 0.1% larger than the arc length of the surface. In the plate-forming process, when choosing a forming method with compressive inherent strain, such as the line heating, the initial shape should be slightly larger than the target shape. Conversely, when choosing a forming method with tensile inherent strain, such as roller peening, the initial material should be slightly smaller than the target shape.

In these examples, we can conclude that the method proposed in this paper can effectively perform surface flattening and obtain in-plane strain distributions that are predominantly compressive or tensile, depending on the requirements. With this method, we can perform surface flattening for different forming methods to obtain a more accurate initial shape for forming.

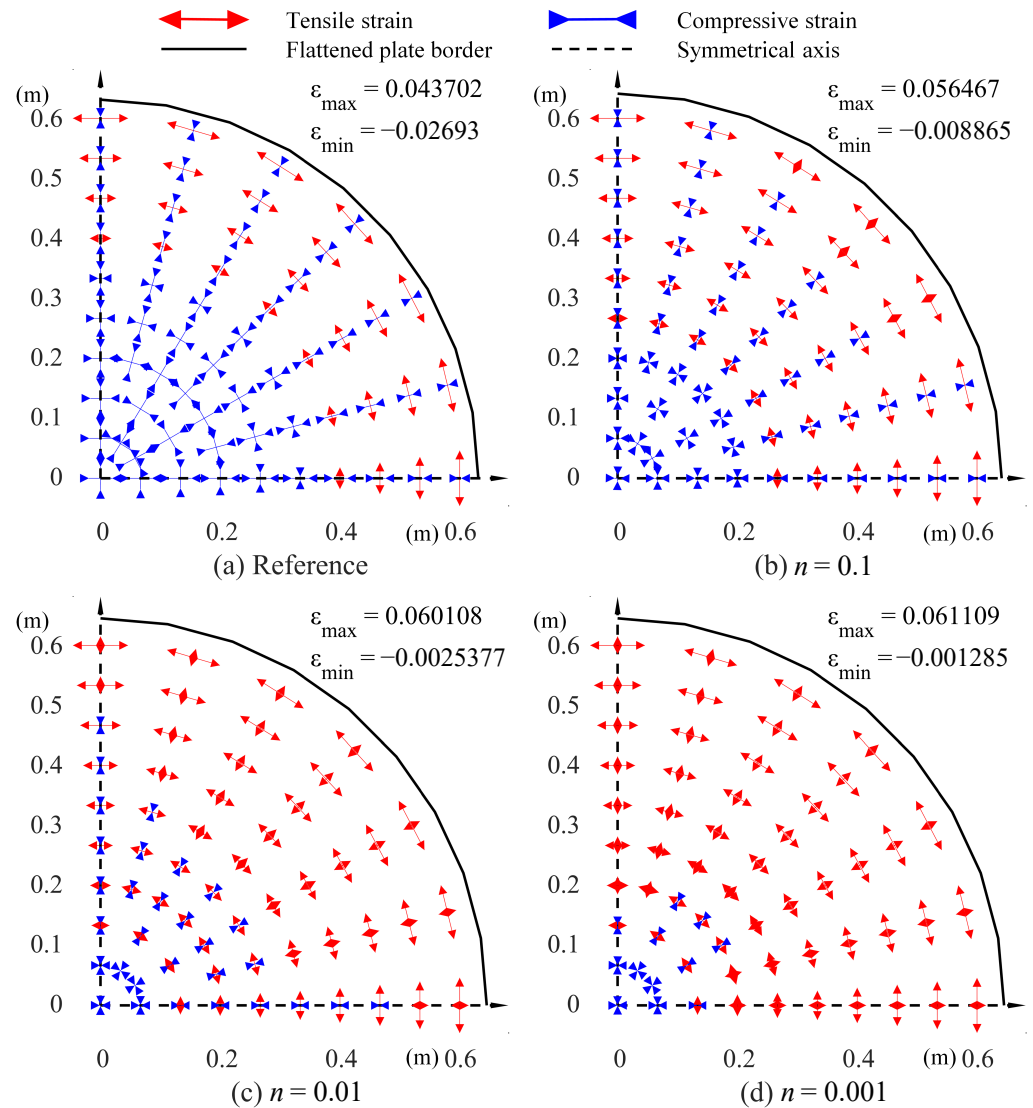


Figure 6. Principal membrane strain vector of spherical cap flattening with dominating tensile strain (a) reference, (b) $n = 0.1$, (c) $n = 0.01$, (d) $n = 0.001$.

3.2. Pillow and Saddle Shape

Pillow- and saddle-shaped surfaces are typical ship hull plate shapes. The surface flattening is essential in the plate-forming process. This section gives examples of pillow-shape and saddle-shape surface flattening. The following Figure 9 shows the shapes of the surface. The plate size is $2\text{ m} \times 1\text{ m} \times 20\text{ mm}$.

We perform the surface-flattening calculation for pillow and saddle shapes under the following four conditions:

- Using the general steel constitutive relations to produce tensile strain without constraint as a reference result,
- Using a constructed constitutive relation to produce tensile strain dominant, setting factor $n = 0.001$,

- Using a constructed constitutive relation to produce tensile strain in X direction dominant, setting factors $n = 0.001$ and $m = 1000$,
- Using a constructed constitutive relation to produce tensile strain in Y direction dominant, setting factors $n = 0.001$ and $m = 1000$.

We use the surface-flattening results without constraint as reference results. Then, Figures 10 and 11 compare the results of membrane strain distribution. According to the symmetry of the target shape, only a quarter region of the results is shown. Moreover, we compare the shapes flattened in Table 2.

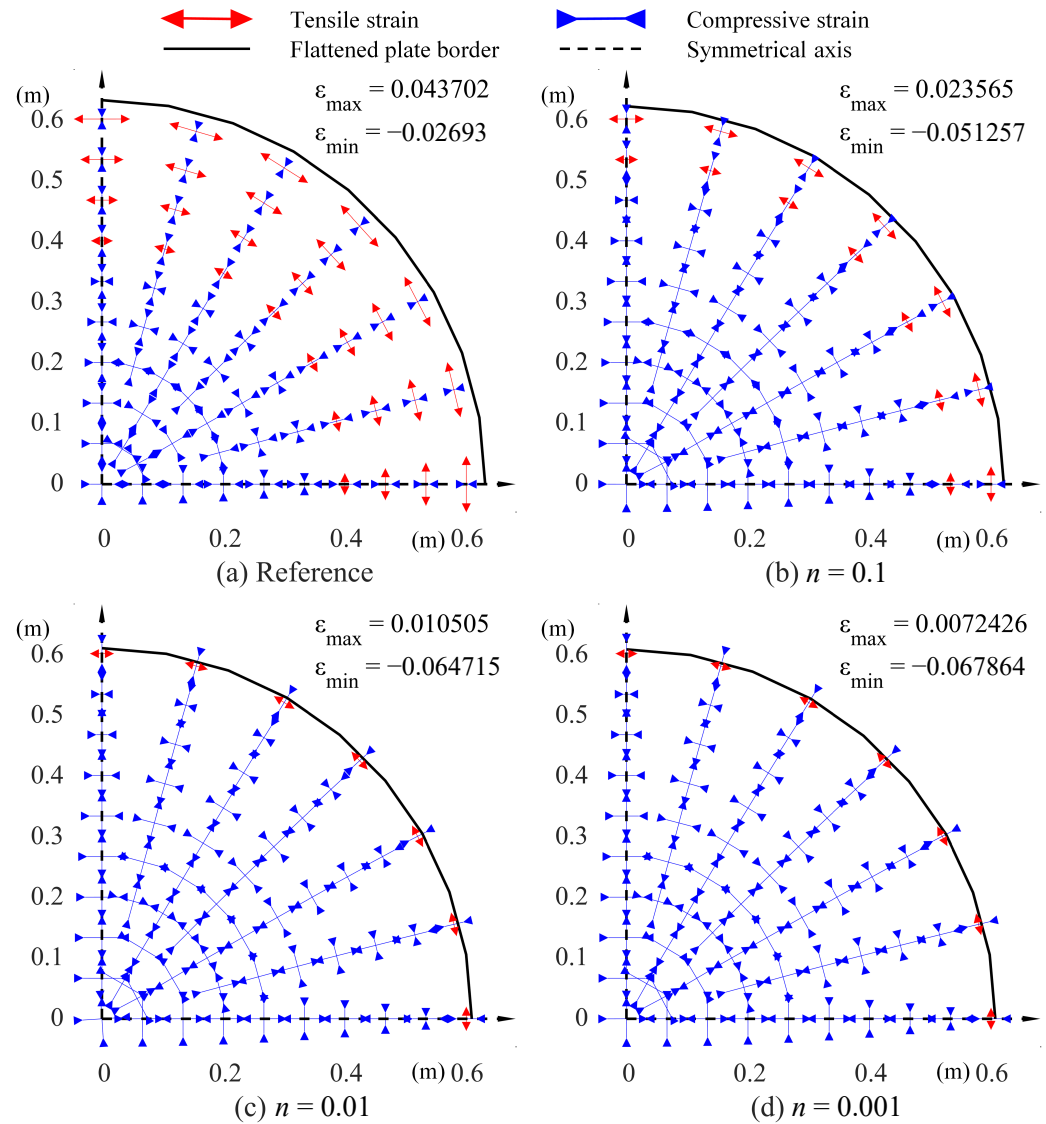


Figure 7. Principal membrane strain vector of spherical cap flattening with dominating compressive strain (a) reference, (b) $n = 0.1$, (c) $n = 0.01$, (d) $n = 0.001$.

For pillow shape surfaces, in the reference results, the membrane strain near the edges is predominantly tensile, and the membrane strain in the region near the center is predominantly compressive. When a constraint is applied so that the strain is predominant tensile in the whole region, the compressive strain is much smaller than the tensile strain. However, the direction of the principal strain is not uniform on the whole plate. Although the maximum tensile strain increases, forming can be performed singly. When the direction of the principal strain is further constrained, the membrane strain is mainly tensile along the X direction. There is a minor compressive strain near the X axis and a slight increase in tensile strain in the area far from the X axis. At this time, the direction of the principal

strain is more regular and more conducive to forming. When constraining the principal strain along the Y direction, there is a more significant tensile strain in the area far from the Y axis. Meanwhile, the maximum tensile strain value in this situation is significantly larger than in the first two cases. Comparing the above results, we can conclude that plate forming by applying membrane strain along the X direction is a more easily achievable forming method.

Table 2. Comparison of pillow- and saddle-shape flattening results.

	Case	Edge Length X Direction (m)	Edge Length Y Direction (m)	Maximum Membrane Strain (10^{-3})	Minimum Membrane Strain (10^{-3})
Pillow	Reference	2.0366	1.0034	4.37	-2.32
	Tensile strain	2.0394	1.0045	6.17	-0.14
	Tensile strain X dir	2.0427	1.0019	6.86	-0.12
	Tensile strain Y dir	2.0325	1.0161	22.39	-0.93
Saddle	Reference	1.9989	1.0054	1.56	-2.87
	Tensile strain	2.0025	1.0065	3.96	-0.17
	Tensile strain X dir	2.0023	1.0064	4.67	-0.24
	Tensile strain Y dir	2.0006	1.0053	10.27	-1.74

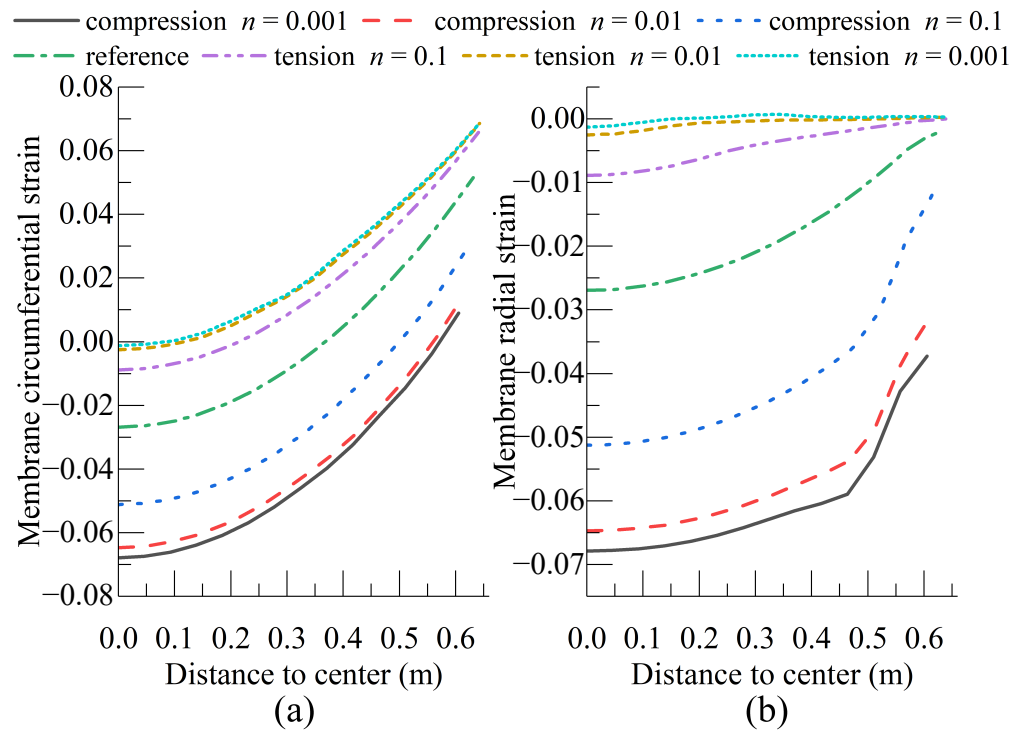


Figure 8. Comparison of principal membrane strain in spherical cap-flattening (a) circumferential strain, (b) radial strain.

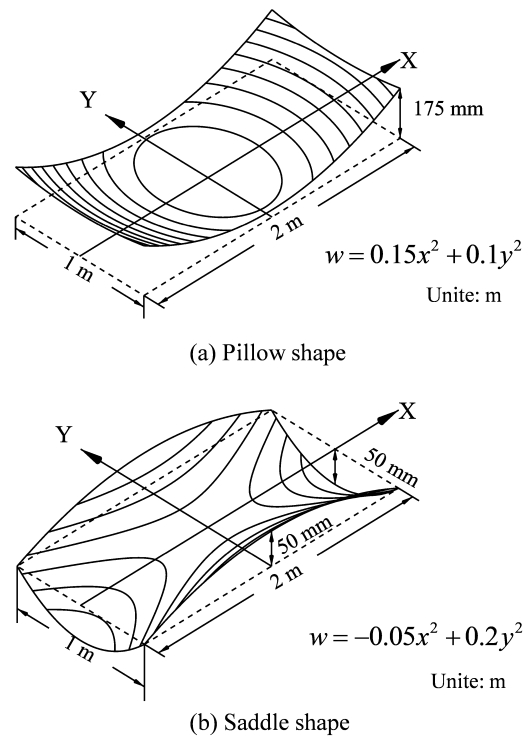


Figure 9. Surface shape with contour line (a) pillow shape, (b) saddle shape.

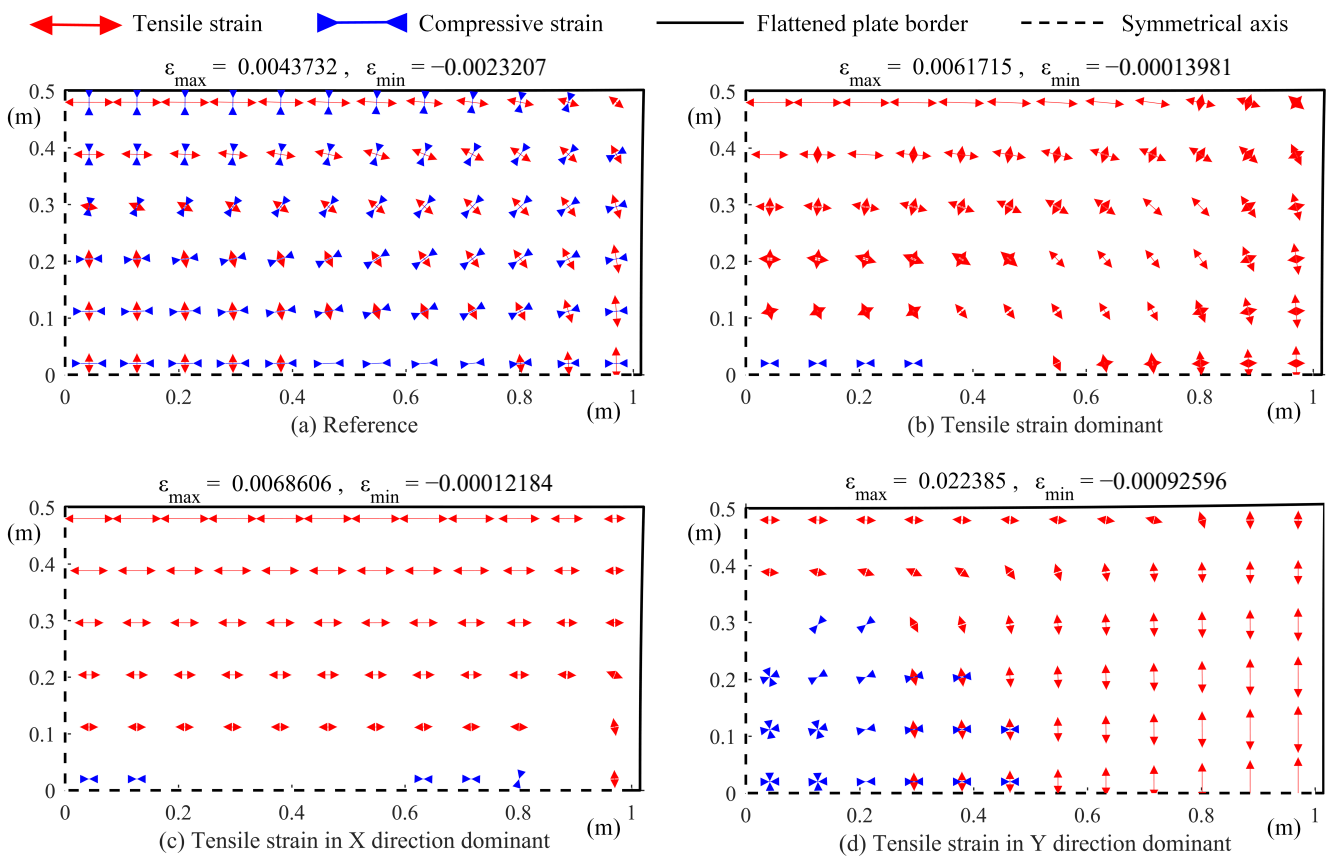


Figure 10. Principal membrane strain vector of pillow-shape flattening (a) reference, (b) tensile strain dominant, (c) tensile strain in X direction dominant, (d) tensile strain in Y direction dominant.

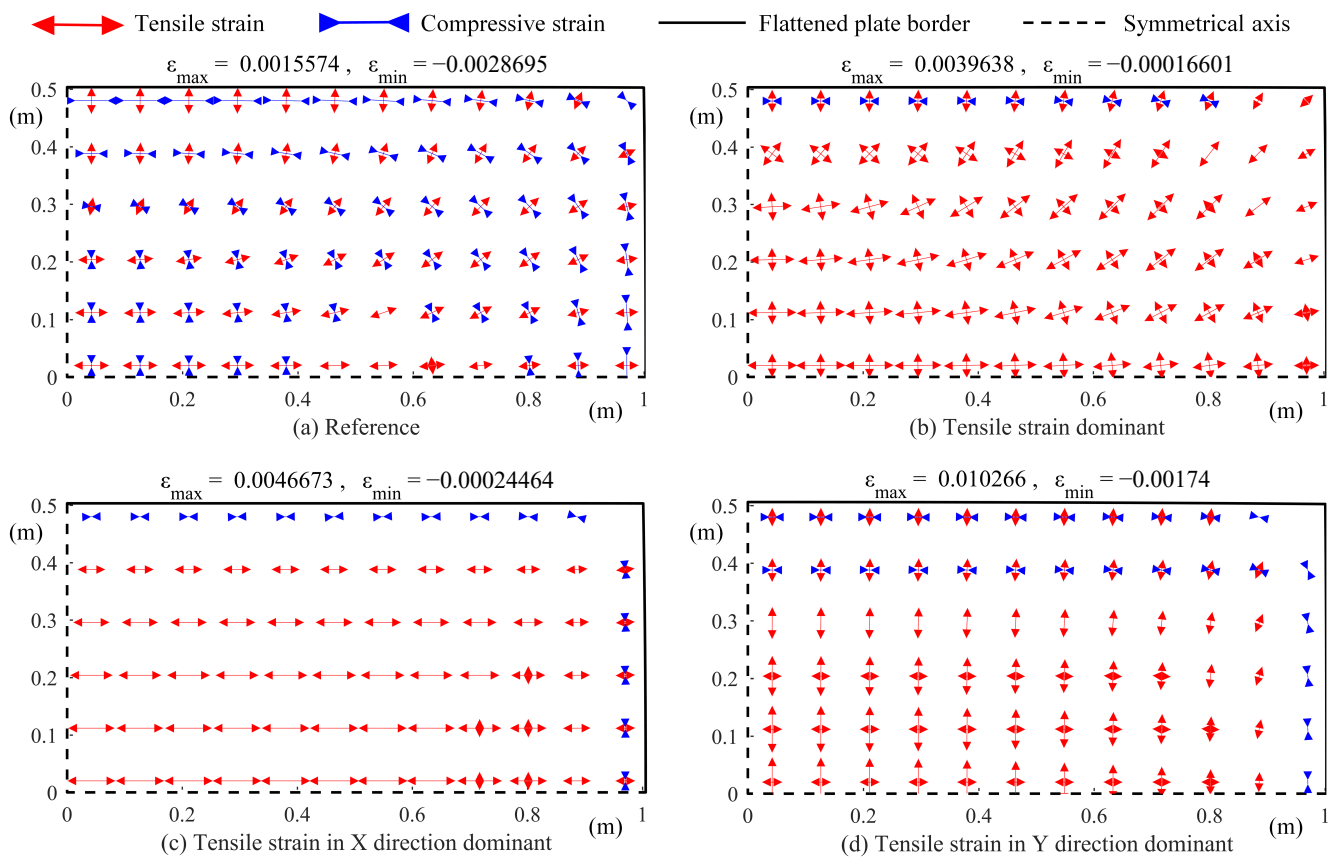


Figure 11. Principal membrane strain vector of saddle-shape flattening (a) reference, (b) tensile strain dominant, (c) tensile strain in X direction dominant, (d) tensile strain in Y direction dominant.

Correspondingly, the saddle-shape surface-flattening has the central part stretched, and the edge part compressed. When the membrane strain is constrained, the area of tensile strain increases, and the maximum value of tensile strain increases. At this point, the compressive strain remains only in part very close to the edges. Therefore, it is numerically much smaller than the tensile strain. When further constraining the strain only along a single direction, again, there is a more considerable tensile strain near the center, decreasing with increasing distance to the center. The strain at the edges is much smaller than at the center. Comparing constraining along the X direction with the Y direction, the strain produced when constrained along the Y direction is significantly larger than when constrained along the X direction.

The flattened shape differs when different constraint methods are used for surface flattening. For example, when the tensile strain is increased by applying constraints, the resulting flattened shape increases slightly. Different initial shapes should be used when forming the same target shape using different forming methods.

Based on the above examples, we can conclude that the proposed method can constrain the principal strain direction while constraining the strain state to obtain the membrane strain distributed along a specific direction. We can perform surface flattening differently to obtain different processing schemes for a shape.

3.3. Comparison and Verification

Ueda [2] proposed a method that uses iterations of applying a specific inherent strain to obtain an orthogonal strain distribution. This section verifies the strain distribution obtained by comparing it with the previous methods. The target surface is a saddle-shaped surface, as shown in Figure 12.

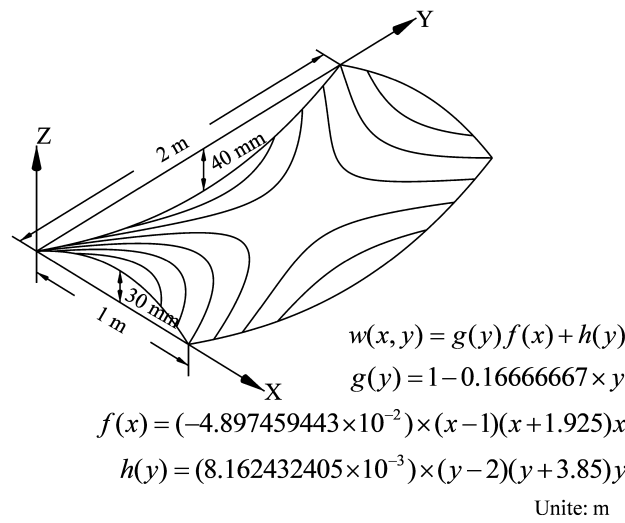


Figure 12. Shape of a curved plate.

Using the surface-flattening method in this paper, we can also obtain the orthogonal inherent strain distribution required for forming. Figure 13 gives the obtained strain distribution. Table 3 shows the comparison of the flattened strain. The maximum and minimum values of the bending strain are 2.67×10^{-3} and -9.67×10^{-4} , respectively, and the minimum membrane strain becomes -2.05×10^{-3} . The strain magnitude is very close to the result of Ueda, and the distribution form is approximately the same.

Table 3. Result comparison.

	Ueda's Result	This Paper
Maximum bending strain	2.98	2.82
Minimum bending strain	-9.77	-9.67
Minimum membrane strain	-2.07	-2.06
Mises stress with inherent strain distributed (MPa)	9.28	1.37

Then, we apply the strain distribution to a freely deformed flat plate as inherent strain. Table 4 gives a comparison of the deformation results. It shows that the error from the maximum deformation is about 0.77%. The deformed shape is very close to the target shape. Figure 14 gives the resulting Mises stress. It shows that the maximum value of Mises stress is 1.37 MPa, slightly smaller than Ueda's calculated result. The high stress values on the corners may be caused by asymmetry of the target shape. Moreover, the Mises stress is less than 0.5 MPa in most areas of the plate, so we can assume that the inherent strain applied does not generate secondary elastic deformation at this time. The strain distribution we obtained satisfies the compatibility condition and is usable for processing. Furthermore, since the relationship between deformation and strain during the flattening process is determined by the compatibility condition, independent of the material constitutive relationship, the strain distribution must be compatible.

From this comparison, we can conclude that our proposed method can obtain the membrane strain distribution for forming process and satisfy the compatibility condition. Compared with the previous method, this method does not require iterative calculations, and the results can be obtained by one static calculation with high computational efficiency.

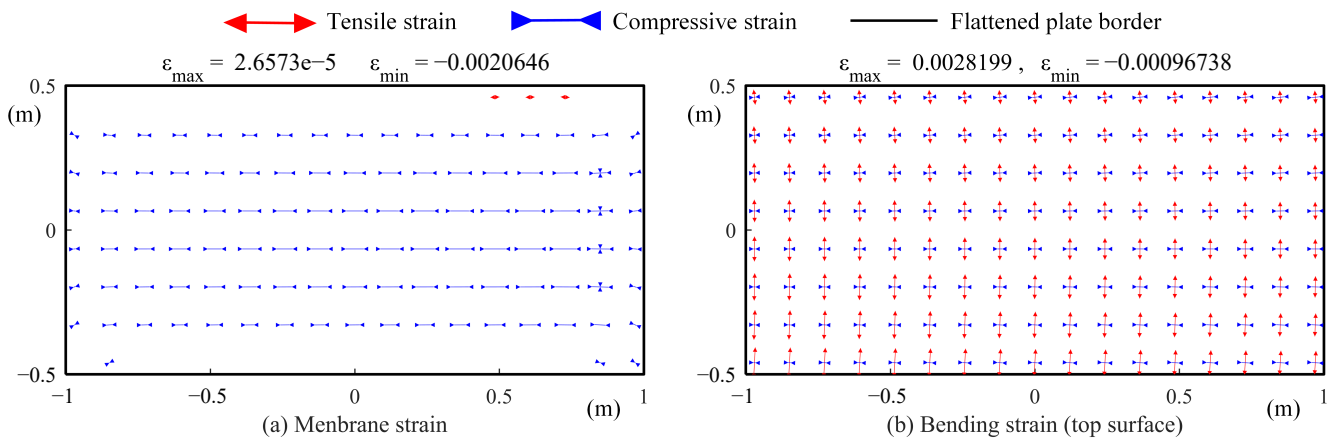


Figure 13. Orthogonal inherent strain using the proposed method (a) membrane strain, (b) bending strain (top surface).

Table 4. Geometry error comparison.

	Desired Shape	Distributed Inherent Strain (Ueda's Result)	Distributed Inherent Strain (This Paper)
w_{max} (mm)	30.0	29.98	29.77
w_{min} (mm)	-40.0	-39.64	-40.00

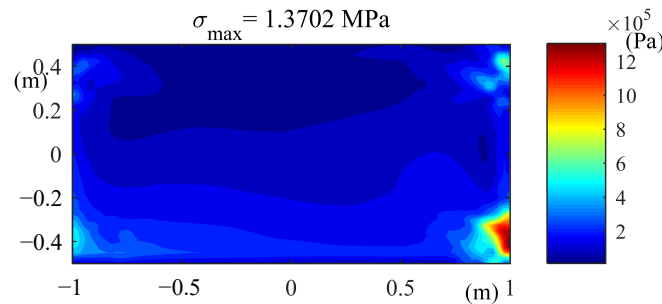


Figure 14. Mises stress with inherent strain applied to a free plate.

4. Application

The forming of double-curved plates is an essential process in shipbuilding. Curved surface flattening helps find the initial shape of double-curved plates and design the forming plan. This section gives an example of applying a surface-flattening calculation in engineering. We can calculate the surface flattening of the target shape to obtain the initial flat plate shape and the inherent strain distribution desired during the forming process. We can then formulate a processing plan according to the required inherent strain distribution and determine the processing path and parameters. The following steps describe the entire process of the forming experiment.

- Flatten the target surface according to the above method with constraint, and obtain the inherent strain distribution required.
- Design the forming plan according to the inherent strain distribution. Lay out the rolling line in the direction perpendicular to the bending strain and the heating line in the area of high membrane strain. Select processing parameters according to the processing parameter database.
- Carry out the forming process simulation to verify the forming plan.
- Carry out the forming experiment, and compare it with the target shape.

4.1. Surface Flattening and Process Plan

Various methods form a ship hull’s double-curved outer plats. Ueda [2] proposed using electromagnetic induction line heating for plate forming. In the line-heating process, the material is constrained from the surrounding area when it expands by heat, resulting in compressive plastic strain. Due to the uneven heating on the upper and lower surfaces of the plate, temperature differences cause different compressive strain. The deformation caused by line heating is mainly membrane shrinkage. Shim [21] proposed using a line array roll set for curved plate forming. In this method, three-point bending is used to generate bending plastic strain in the plate, and the membrane deformation of the plate is small. Chang [4] proposed a way to process curved plates using arc-shaped rollers. In this method, the shape of the rollers is controlled to provide different pressure at each part of the plate, and the plate produces membrane tensile deformation. Zhao [6] proposed to combine line heating and roller bending for plate forming. A richer deformation can be produced by combining different forming tools.

We choose a pillow shape surface as the target shape and use a combination of line heating [22] and concave–convex roller bending [6,23] to perform the forming process. First, the surface flattening calculation is performed for the target shape. The membrane strain should be constrained because the line heating process can only produce compressive membrane strain. The membrane strain in the surface flattening calculation should be mainly tensile. Based on the surface-flattening calculation results, we can obtain the bending strain and membrane strain distribution required in the forming process, as shown in Figure 15 below. According to the inherent strain distribution, we can decide forming position. Based on the inherent strain magnitude, we can obtain the forming parameters by referring to a parameter database [23]. We take the following processing scheme. First, we use roller bending to apply bending strain along the X direction. Then, line heating applies the compressive membrane strain on the sides of the plate. Due to the simultaneous action of bending strain and membrane strain, we process the flat plate into the target pillow shape. For the roller bending process, the downward depth of the roller bending is set to 3 mm and repeated twice. For the line heating process, the power of the heat source is 60 kW, and the speed is ten mm/s; repeat four times. The arrangement of the processing line is shown in Figure 16.

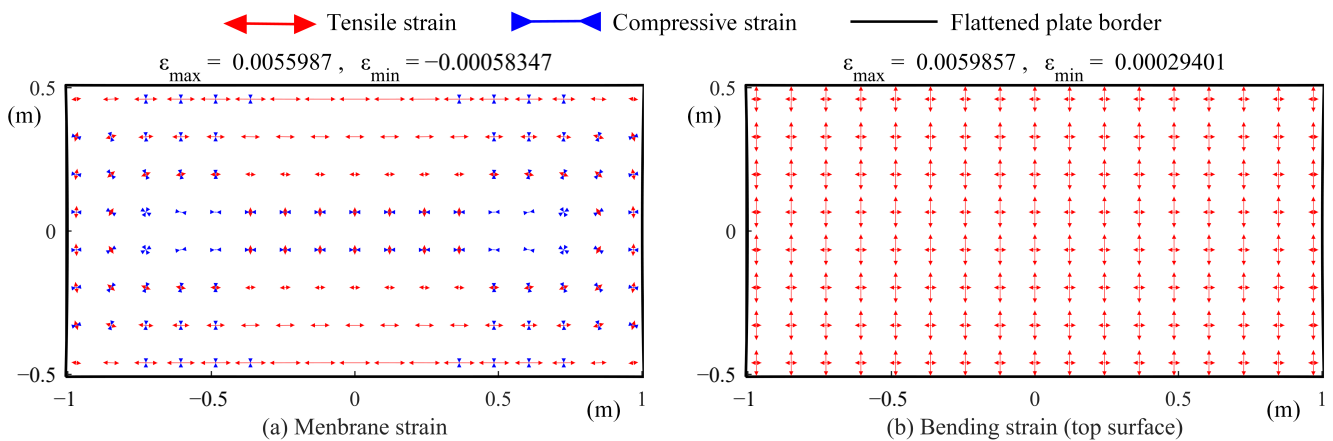


Figure 15. Principal inherent strain distribution desired in forming process (a) membrane strain, (b) bending strain (top surface).

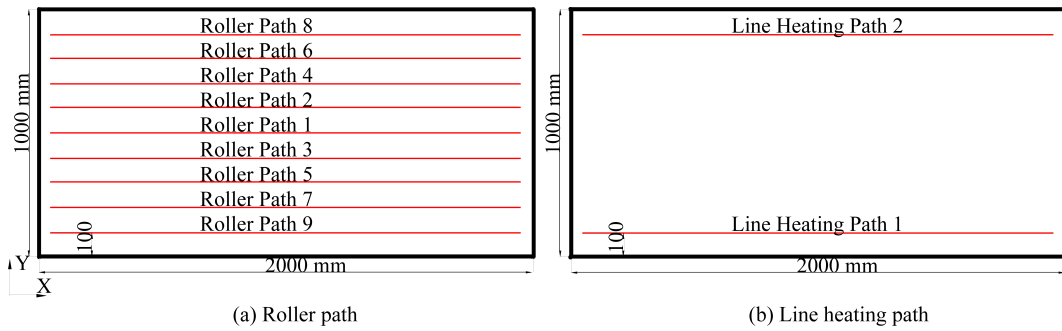


Figure 16. Process line schematic (a) roller path (b) line heating path.

4.2. Finite Element Simulation

We use a computer to simulate the forming process according to the above scheme. We use ABAQUS software [24] for finite element simulations. First, we establish the finite element model of the plate. The mesh size is set to 10 mm. We use four-node reduced integral shell elements (S4R) in the deformation calculation and use four-node heat transfer elements (DS4) in the heat-transfer calculation, and the material properties refer to Dong’s [22,23] study. In the roller-bending process, the upper and lower rollers are modeled as rigid bodies, as shown in Figure 17a,b. The roller processing is a quasi-static process. In the line-heating process, the surface heat source model is established according to the shape of the induction heating heat source, and then the heat transfer process of forming is simulated. The heat source is simplified to a surface heat-flow density in the heat-transfer calculation. Thus the complex coupled thermal electromagnetic simulation is avoided. A subroutine DFLUX is used in ABAQUS to realize the heat source movement along a straight line on the surface of the plate and set the convection and radiation heat-dissipation conditions with the external environment [24]. The temperature field obtained from the heat-transfer calculation is then used as a load for the elastic-plastic mechanical calculation to obtain the deformation resulting from the line-heating process. In the mechanical calculation, the boundary conditions constrain only the three corner-point constraints of the rigid body displacement.

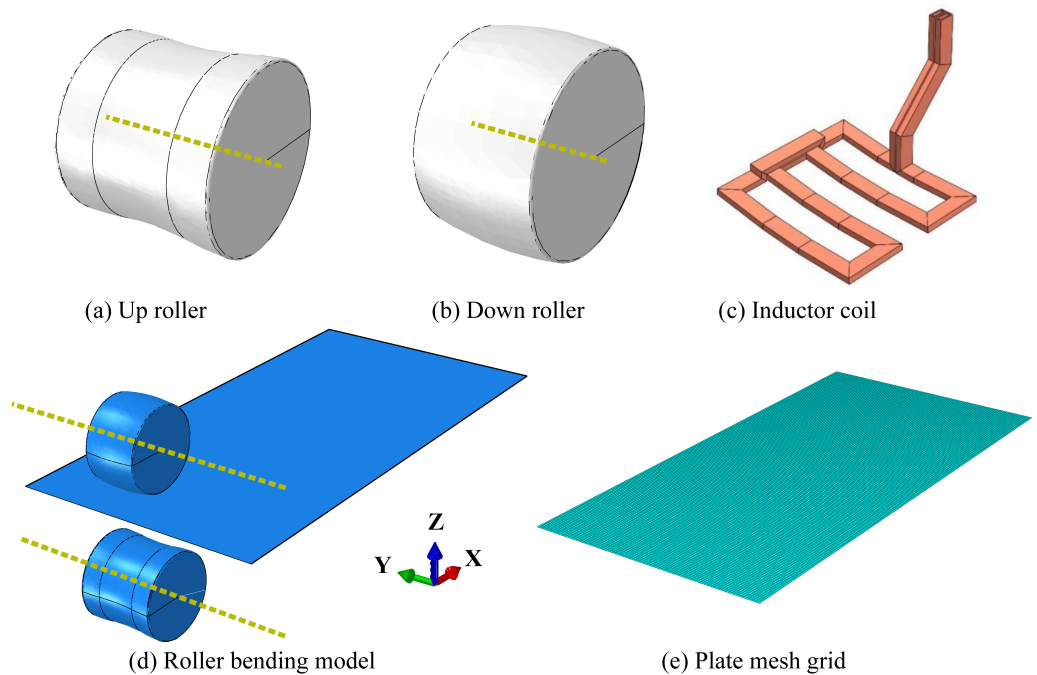


Figure 17. Finite element model (a) up roller, (b) down roller, (c) inductor coil, (d) roller-bending model, (e) plate mesh grid.

4.3. Experiment

We performed the above process on a plate-forming experimental processing platform [6]. The experimental platform comprises hydraulic rollers, induction heating system, servo positioning system, laser-scanning measurement system, and other assistant parts. The platform is shown in Figure 18. It can be combined or used alone for roller bending and induction line heating to form curved plates. We carried out tests according to the above processing plan.

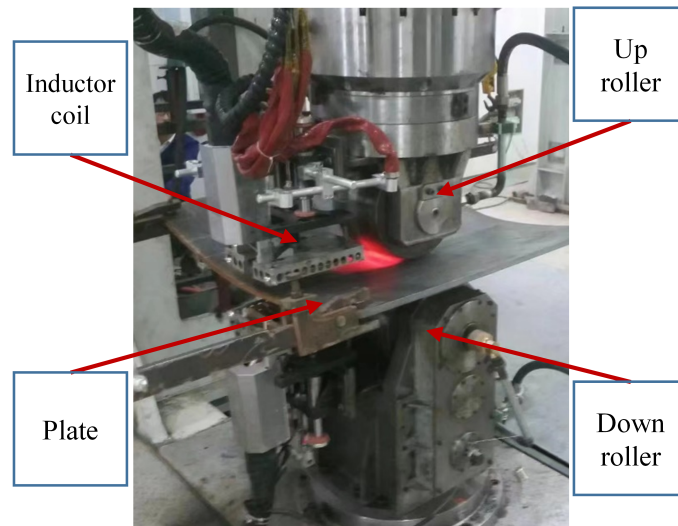


Figure 18. Experimental platform.

4.4. Results and Discussion

Figure 19 shows the out-of-plane deformation contour diagram of the plate in the simulation and the deformation measurement results in the processing test. Figure 20 compares the deformation along the longitudinal and transverse cross-sections with the target shape. Both show that the processing scheme can form the flat plate to the target pillow shape. As shown in Figure 20b, there is an error of about 10 mm in the long side direction. The error may be because the actual processing cannot strictly produce the strain distribution obtained by unfolding, and further research should be carried out to improve forming accuracy. Figure 21 shows the actual strain produced during the forming process. Compared with the strain distribution obtained by flattening the target shape, the strain distribution resulting from forming is similar to the desired strain distribution. This result shows that the target shape can be formed by applying the strain distribution obtained in surface flattening.

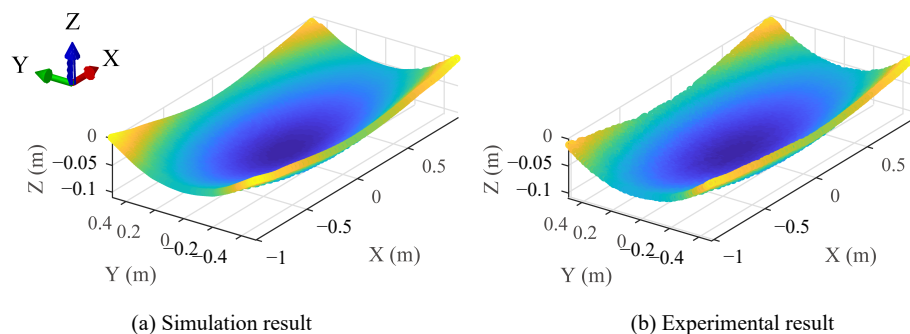


Figure 19. Shape of deformed plate (a) simulation result, (b) experimental result.

With this example, we can conclude that applying the surface-flattening method proposed in this paper can guide the forming scheme in the surface forming process. Furthermore, the surface-flattening method can be flexibly adjusted according to different forming methods.

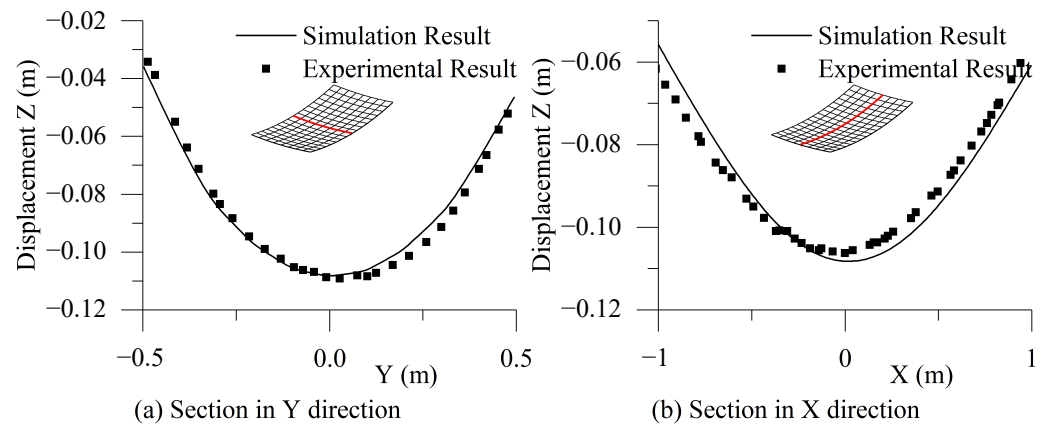


Figure 20. Displacement in Z direction along section (a) section in Y direction, (b) section in X direction.

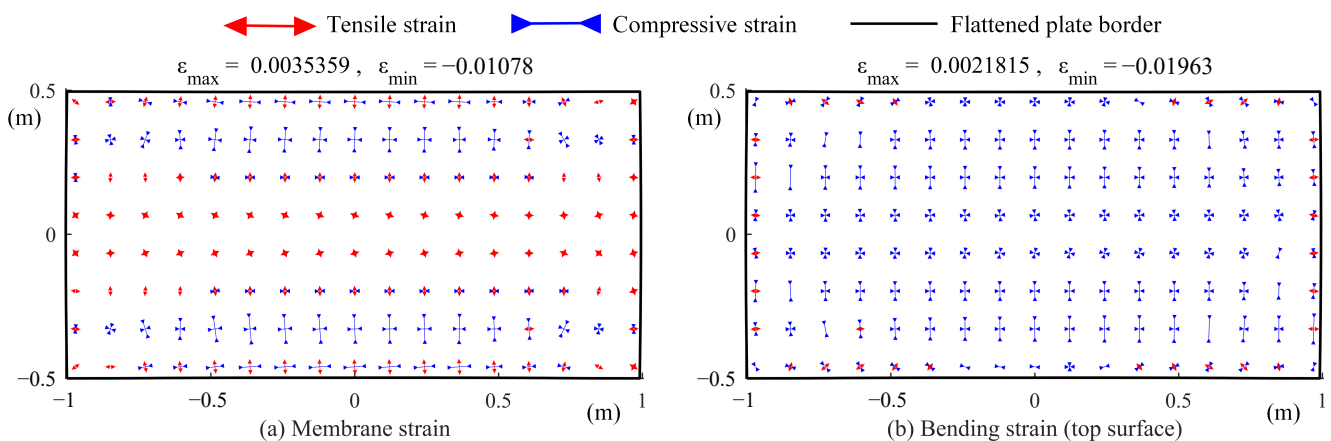


Figure 21. Principal strain vector produced in forming process (a) membrane strain, (b) bending strain (top surface).

5. Conclusions

This paper proposes a method for surface-flattening calculation using the finite element method. The membrane strain can be constrained by modifying the material constitutive relationship. This method can obtain membrane strain dominated by tensile or compressive strain. According to the numerical examples, this method can efficiently realize the curved surface-flattening process and obtain the strain distribution and the initial shape. Changing the value of the relaxation coefficient n can control the proportion of the tensile and compressive strain regions. Furthermore, the direction of the principal strain can also be constrained to make the membrane strain distribution regular. Compared with other strain flattening methods, this can obtain a more accurate strain distribution and save computing resources. The strain distribution obtained by this calculation method can guide curved surface forming in the forming experiment.

Author Contributions: Conceptualization, L.C. and Y.Z.; methodology, L.C. and Y.Z.; software, L.C.; validation, L.C. and Z.W.; investigation, H.Y. and Z.W.; writing—original draft preparation, L.C.; writing—review and editing, Y.Z., H.Y. and Z.W.; visualization, L.C. All authors have read and agreed to the published version of the manuscript.

Funding: This work was supported by the Ministry of Science and Technology of the People's Republic of China (Grant No.: 2012DFR80390).

Institutional Review Board Statement: Not applicable.

Informed Consent Statement: Not applicable.

Data Availability Statement: Not applicable.

Conflicts of Interest: The authors declare no conflict of interest.

References

- Shen, H.; Wang, H.; Zhou, W. Process modelling in laser forming of doubly-curved sheets from cylinder shapes. *J. Manuf. Process.* **2018**, *35*, 373–381. [[CrossRef](#)]
- Ueda, Y.; Murakawa, H.; Rashwan, A.M.; Kamichika, R.; Ishiyama, M.; Ogawa, J.I. Development of Computer Aided Process Planning System for Plate Bending by Line-Heating (Report IV): Decision Making on Heating Conditions, Location and Direction (Mechanics, Strength & Structural Design). *Trans. JWRI* **1993**, *22*, 9.
- Ueda, Y.; Murakawa, H.; Ma, N. *Welding Deformation and Residual Stress Prevention*; Elsevier Butterworth-Heinemann: Burlington, NJ, USA, 2012. [[CrossRef](#)]
- Chang, X.; Fu, W.; Li, M.; Wang, X. The flexible rolling process of three-dimensional curved parts using an auxiliary plate based on rigid arc-shaped rollers. *Int. J. Adv. Manuf. Technol.* **2021**, *116*, 1103–1113. [[CrossRef](#)]
- Ueda, Y.; Murakawa, H.; Rashwan, A.M.; Okumoto, Y.; Kamichika, R. Development of Computer Aided Process Planning System for Plate Bending by Line Heating (Report I): Relation between the Final Form of Plate and the Inherent Strain (Mechanics, Strength & Structural Design). *Trans. JWRI* **1991**, *20*, 275–285.
- Zhao, Y.; Yuan, H.; Tang, G.; Dong, H.; Hu, C.; Yan, J. Automatic Integral Forming Method for Double-Curvature Plate of Ship. The United States Patent 14/584943, 5 September 2017.
- Wang, X.; Shi, Y.; Guo, Y.; Wang, Q. Design of 3D surface laser forming process. *J. Manuf. Process.* **2022**, *73*, 306–315. [[CrossRef](#)]
- Ryu, C.; Shin, J.G. Optimal Approximated Unfolding of General Curved Shell Plates Based on Deformation Theory. *J. Manuf. Sci. Eng.* **2006**, *128*, 261–269. [[CrossRef](#)]
- Zhang, S.; Liu, C.; Wang, X. An optimal flattening algorithm for ship hull plate fabricated by thermal forming. *J. Mar. Sci. Technol.* **2018**, *24*, 134–151. [[CrossRef](#)]
- Lan, H.; Liu, C.; Nie, X. Multi-Objective Optimization Model for Expansion Method of Three-Dimensional Curved Hull Plate. *Shanghai Jiaotong Daxue Xuebao/J. Shanghai Jiaotong Univ.* **2020**, *54*, 1101–1107. [[CrossRef](#)]
- Chapelle, D.; Bathe, K.J. *The Finite Element Analysis of Shells-Fundamentals*, 2nd ed.; Computational Fluid and Solid Mechanics, Springer: Berlin/Heidelberg, Germany, 2011. [[CrossRef](#)]
- Dvorkin, E.N.; Bathe, K.J. A continuum mechanics based four-node shell element for general nonlinear analysis. *Eng. Comput.* **1984**, *1*, 77–88. [[CrossRef](#)]
- Ambartsumyan, S.A. Basic equations and relations in the theory of anisotropic bodies with different moduli in tension and compression. *Inzh. Zhur. MTT* **1969**, *3*, 51–61.
- Ambartsumyan, S.A. *Elasticity Theory of Different Moduli*; China Railway Publishing House: Beijing, China, 1986.
- Tabaddor, F. Two-Dimensional Bi-Linear Orthotropic Elastic Materials. *J. Compos. Mater.* **2016**, *3*, 725–727. [[CrossRef](#)]
- Jones, R.M. Buckling of circular cylindrical shells with different moduli in tension and compression. *AIAA J.* **1971**, *9*, 53–61. [[CrossRef](#)]
- Jones, R.M. *Mechanics of Composite Materials*; McGraw-Hill: New York, NY, USA, 1975.
- Itskov, M. *Tensor Algebra and Tensor Analysis for Engineers (Second Edition): With Applications to Continuum Mechanics*; Springer: Berlin/Heidelberg, Germany, 2009; pp. 1–247. [[CrossRef](#)]
- He, X.t.; Zheng, Z.l.; Sun, J.y.; Li, Y.m.; Chen, S.l. Convergence analysis of a finite element method based on different moduli in tension and compression. *Int. J. Solids Struct.* **2009**, *46*, 3734–3740. [[CrossRef](#)]
- Bathe, K.J.; Dvorkin, E.N. A four-node plate bending element based on Mindlin/Reissner plate theory and a mixed interpolation. *Int. J. Numer. Methods Eng.* **1985**, *21*, 367–383. [[CrossRef](#)]
- Shim, D.; Yang, D.; Chung, S.; Han, M. Optimization of forming steps in the incremental forming of twisted shapes using a line array roll set (LARS). *Int. J. Precis. Eng. Manuf.* **2010**, *11*, 715–723. [[CrossRef](#)]
- Dong, H.; Zhao, Y.; Yuan, H.; Hu, X.; Yang, Z. A Simplified Calculation Method of Heat Source Model for Induction Heating. *Materials* **2019**, *12*, 2938. [[CrossRef](#)]
- Dong, H. Scheme Generating Method and Experiment Verification of Cold and Hot Loading for Forming Curved Plates of Ship. Ph.D. Thesis, Huazhong University of Science & Technology, Wuhan, China, 2020.
- ABAQUS. *ABAQUS Analysis User's Manual*; ABAQUS: Providence, RI, USA, 2015.

Disclaimer/Publisher's Note: The statements, opinions and data contained in all publications are solely those of the individual author(s) and contributor(s) and not of MDPI and/or the editor(s). MDPI and/or the editor(s) disclaim responsibility for any injury to people or property resulting from any ideas, methods, instructions or products referred to in the content.